International Journal of Rotating Machinery
1998, Vol. 4, No. 3, pp. 175–188
Reprints available directly from the publisher
Photocopying permitted by license only

Heat/Mass Transfer Distribution in a Rotating Two-Pass Square Channel

Part I: Regional Heat Transfer, Smooth Channel

C.W. PARK, M. KANDIS and S.C. LAU*

Department of Mechanical Engineering, Texas A&M University, College Station, TEXAS 77843-3123

(Received 22 January 1997; In final form 13 February 1997)

Naphthalene sublimation experiments have been conducted to examine the effect of rotation on the regional heat/mass transfer distribution for turbulent air flow in a rotating smooth two-pass square channel that has a 180° turn with sharp corners. The Reynolds number ranges from 5,500 to 14,500 and the rotation number goes up to 0.24. The test channel models the first two passes of serpentine internal cooling passages of gas turbine blades. Flow around a sharp turn causes larger heat/mass transfer increase in the turn and in the second pass than flow around a smooth turn. In the first pass with radially outward flow, rotation increases the heat/mass transfer on the trailing wall and decreases the heat/mass transfer on the leading wall. The reversed trend in the second pass with radially inward flow is evident only after four hydraulic diameters downstream of the turn exit. With rotation, there is an abrupt increase of the regional heat/mass transfer in the upstream portion of the turn on the leading wall. The regional heat/mass transfer on the trailing wall, however, increases along the streamwise direction in the turn, as in the stationary channel case. In the turn and immediately downstream of the turn, the shape of the heat/mass transfer distribution in a rotating channel is invariant over the range of rotation number studied. In a rotating channel, decreasing the Reynolds number increases the heat/mass transfer on the trailing wall and decreases that on the leading wall in the first pass, and increases the heat/mass transfer on both walls in the turn and immediately downstream of the turn.

Keywords: Heat and mass transfer, Rotating two-pass square channel, Sublimation method

INTRODUCTION

The objective of this investigation is to study the effect of rotation on the heat transfer distribution in serpentine cooling passages in modern gas turbine blades. The geometries of these cooling passages, with their consecutive straight sections and sharp turns, significantly affect the flow and heat transfer distributions. In and around the turn regions, centrifugal forces give rise to secondary flows that increase the heat transfer variations in the turn and in the downstream straight section.

* Corresponding author.

Increasing the heat transfer is beneficial, but large temperature gradients may produce excessive thermal stresses. Coriolis and buoyancy forces resulting from rotation also produce secondary flows throughout the cooling passages. Thus, the flows in these passages are highly three-dimensional and extremely difficult to predict.

In this study, naphthalene sublimation experiments are conducted with a rotating two-pass square channel. Since the test channel walls and the air that flows through the test channel are both at room temperature, there is no density variation in the test channel due to temperature variation in the flow field. Thus, buoyancy effect in actual turbine blade cooling channels is not simulated. It may also be shown that the naphthalene vapor partial pressure and concentration at the test channel walls are very small, such that the maximum density variation in the naphthalene vapor-air mixture (relative to the density of the mixture) that flows through the test channel is only about 5×10^{-4}. Therefore, the results to be presented will illustrate only the effects of Coriolis force and turn-induced secondary flow on the local heat/mass transfer distribution. These results will not only enhance understanding of the momentum and thermal transport processes that take place in internal flows with rotation, but will also enable the turbine engine designer to develop improved numerical codes to determine local temperature and thermal stress distributions in turbine blades under actual operating conditions. This information is critical if newer gas turbines are to be operated at ever higher temperatures for maximum efficiencies.

LITERATURE REVIEW

A significant amount of experimental data is available in the literature on heat and mass transfer and pressure drop for turbulent flows in stationary multipass channels with smooth walls or rib-roughened walls, for instance, Burggraf [1970], Webb et al. [1971], Donne and Meyer [1977], Han et al. [1988, 1991], Lau et al. [1991a, 1991b, 1991c], and Kukreja et al. [1993]. Metzger and Sahm [1986] and Fan and Metzger [1987] studied the effect of channel geometry on the heat transfer in smooth rectangular channels with a sharp 180° turn whose walls were maintained at a uniform temperature. Their regionally averaged heat transfer coefficients showed highest heat transfer immediately downstream of the turn. Chandra et al. [1988] measured the local mass transfer distributions in a stationary multipass square channel with smooth and rib-roughened walls. They also found the local mass transfer coefficient to be higher downstream of the turn than upstream of the turn. In the turn region of their smooth channel, the mass transfer coefficients were also high compared to those before the turn.

Rotation of a channel about a perpendicular axis gives rise to Coriolis and buoyancy forces, the coupling of which creates complex flows that affect the heat transfer distributions throughout the channel. Johnston et al. [1972] and Wagner and Velkoff [1972] examined the effect of rotation on turbulent flow in straight channels. Guidez [1988], Iskakov and Trushin [1985], and Wagner et al. [1991a] studied the effect of rotation on heat transfer. Wagner et al. [1991b] conducted a thorough investigation of the effects of Coriolis and buoyancy forces on the regional heat transfer in a rotating serpentine smooth channel. Their results indicated a dependence of the regional heat transfer on several parameters: the streamwise location, the surface orientation, the main flow direction (inward or outward flow), the Reynolds number, UD/ν, the rotation number, $\Omega D/U$, and a buoyancy parameter, $(\Delta\rho/\rho)(\Omega D/U)^2(R/D)$. Although they could not obtain heat transfer results with zero buoyancy force, the available data were extrapolated to provide predictions for such a condition.

Han et al. [1993] studied the effect of wall temperature variation on the heat transfer in a rotating two-pass square channel with smooth walls. They found that uneven wall temperatures provided increased heat transfer coefficients on all

surfaces. In the case of uniform surface temperature, their results agreed well with those of Wagner et al. [1991b].

Wagner et al. [1991c, 1992] presented comprehensive results for regional heat transfer in a serpentine channel with normal and skewed turbulence promoters on the leading and trailing surfaces. Their data showed that turbulence promoters diminished the effects of Coriolis and buoyancy forces on the regional heat transfer distribution.

In the present investigation, the regional and local heat transfer coefficient distributions in a two-pass square channel with smooth walls, rotating about a perpendicular axis, are determined via the naphthalene sublimation technique. The naphthalene sublimation technique has been used in many previous local heat transfer studies, such as Sogin [1958], Sparrow and Tao [1983], Karni and Goldstein [1990], Chyu [1991], and McMillin and Lau [1994]. Early naphthalene sublimation experiments were summarized and the analogy between heat transfer and mass transfer was discussed extensively in Goldstein and Cho [1995].

EXPERIMENTAL APPARATUS AND PROCEDURE

The test apparatus for the mass transfer experiments consisted of an open flow loop, a two-pass square test channel, and a rotation test rig. The test section was a 1.59 cm by 1.59 cm square channel constructed entirely of aluminum. It had two 11.11 cm long straight sections that were connected by a 180° turn with sharp corners. The distance between the tip of the inner wall and the end wall in the turn, or the tip clearance, was also 1.59 cm. The inner wall was 0.794 cm thick. Thus, the upstream and downstream straight sections were both seven hydraulic diameters long, the turn tip clearance was one hydraulic diameter wide, and the inner wall was one half of a hydraulic diameter thick.

The test section consisted of seven wall segments of various shapes – two Π-shaped principal walls, two inner side walls, two outer side walls, and an end wall. Each wall segment was hollowed out and the resulting cavity was filled with naphthalene in a casting process. After the wall segments were assembled, all interior surfaces of the test section were flat, smooth, and mass transfer active.

The test section was mated to an aluminum, mass transfer inactive, inlet and exit section assembly in an aluminum housing (Fig. 1). The inlet and exit sections were 10 and 20 hydraulic diameters long, respectively. The downstream end of the exit section was affixed to a rotating pipe assembly of the rotation test rig (Fig. 2). The distance from the middle of the test section to the rotation axis was thirty hydraulic diameters. The support cage of the rotation test rig was made of two 1.27 cm thick steel plates and four square steel tubes. Protective steel mesh fencing framed with angle irons outlined the perimeter of the cage. A five-horsepower electric motor with a speed controller powered the system via two pulleys and a belt.

The main components of the open flow loop were a blower, a gate valve, and a calibrated orifice flow meter. During an experiment, room air at 22.4°C was drawn from the air-conditioned laboratory. Upon exiting the flow loop, the air was ducted to the outside of the laboratory. Experiments were performed in the suction mode so that any heat transfer from the blower and from the rotating union to the air occurred far downstream of the test section and would not affect the room temperature air passing through the test section.

To determine the local mass transfer distribution, an electronic depth gage and a microcomputer controlled traversing system with step motors were used to measure the elevation changes at an array of points on the naphthalene surfaces of the two principal walls. A precision electronic balance was used to weigh all seven wall segments before and after an experiment to determine the total rate of mass at which naphthalene entered the air stream and the distribution of the bulk density of naphthalene in the air stream.

The temperatures of the air entering the test section and of the air leaving the rotating union

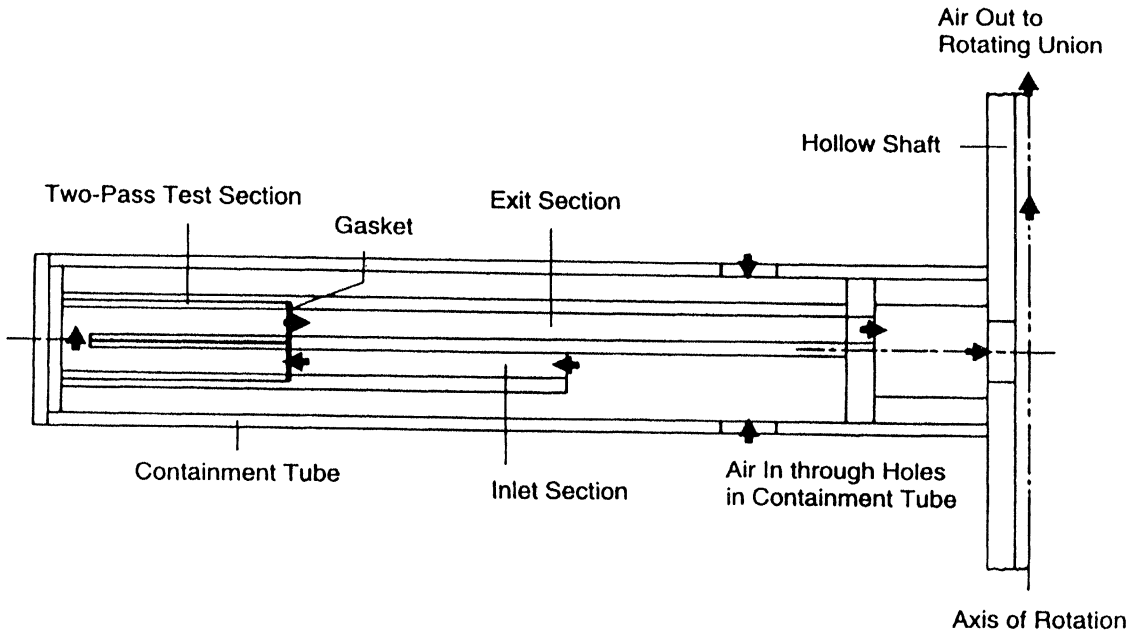

FIGURE 1 Schematic of test apparatus.

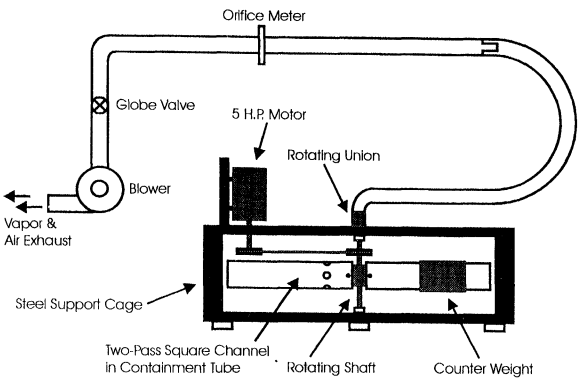

FIGURE 2 Schematic of rotation test rig.

were measured with two calibrated thermocouples along with two digital thermocouple gages. The pressure drop across the orifice and the pressure upstream of the orifice were measured with a U-tube manometer to determine the air flow rate. The rotational speed of the test rig was read with a photo tachometer.

At the beginning of an experiment, the elevations at an array of 312 points on the two Π-shaped principal walls were measured, and the seven wall segments were weighed in a predetermined order. After it was certain that the test section and the rotation assembly were installed properly, the electric motor was switched on. The speed controller was adjusted until the desired rotational speed was reached. The blower was then switched on to allow air to flow through the channel at a predetermined flow rate. While air was allowed to flow through the test section, the air inlet and exit temperatures, the pressure drop across the orifice flow meter, and the rotational speed were recorded periodically.

The test section was removed from the rotation rig. The local elevation distributions on the two principal walls and the weights of all seven wall segments were again measured (with the depth gage and the balance) in the same order as that at the beginning of the experiment. Spanwise averaged (and regionally averaged) mass transfer coefficients and Sherwood numbers on the two principal walls were then calculated from the local mass losses at the 312 points on the two walls.

DATA REDUCTION

The local mass transfer coefficient at each measurement point is evaluated as

$$h_m = \frac{\dot{m}''}{\rho_w - \rho_b} \tag{1}$$

The mass flux is evaluated from the density of solid naphthalene and the change of elevation at the measurement point during a test run after applying the correction that is necessary to account for the mass losses at the beginning and at the end of the test run.

$$\dot{m}'' = \frac{\rho_s \Delta z}{\Delta t} \tag{2}$$

In equation (1), the naphthalene vapor density at the wall, ρ_w, is calculated using the ideal gas law along with the vapor pressure-temperature relation for naphthalene according to Ambrose et al. [1975]. The constant naphthalene vapor density value at the channel walls corresponds to the thermal boundary condition of uniform wall temperature. The bulk density of naphthalene in the air stream, ρ_b, at any streamwise location is calculated as

$$\rho_b = \frac{C_m}{\dot{Q}} \tag{3}$$

The weights of the test section walls at the beginning and at the end of a test run are used to determine the bulk density at the test section exit. Since the bulk density at the inlet of the test section is zero, the bulk density at any streamwise location is determined by linearly interpolating the bulk density values at the inlet and the outlet of the test section.

The local Sherwood number is

$$Sh = \frac{h_m D}{\Lambda} \tag{4}$$

The diffusion coefficient for naphthalene vapor in air, Λ, is calculated with equation (1) in Goldstein and Cho [1995]. The Sherwood number is normalized by the Sherwood number for a corresponding fully developed flow in a stationary smooth tube, which is determined from its heat transfer counterpart, the Dittus-Boelter equation, and the heat/mass transfer analogy.

$$Sh_0 = 0.023\, Re^{0.8}\, Sc^{0.4} \tag{5}$$

The Schmidt number for naphthalene in air is found to be about 2.28. Since the rotation and the turn affect the naphthalene concentration field and the temperature field in the same manner, only through the velocity field in a rotating multipass channel, it is reasonable to employ the following generalized heat/mass transfer analogy.

$$Nu = \left(\frac{Pr}{Sc}\right)^{0.4} Sh \tag{6}$$

thereby,

$$Nu/Nu_0 = Sh/Sh_0 \tag{7}$$

The Reynolds number and the rotation number are defined, respectively, as

$$Re = \frac{\dot{M}}{\mu D} \tag{8}$$

and

$$Ro = \frac{\Omega D}{U} \tag{9}$$

The rotation number may be considered as the strength of the Coriolis force relative to that of the inertia force.

The uncertainty of the local mass transfer coefficient depends on the uncertainties of the local wall and bulk naphthalene vapor densities, and the local mass flux. It is found that a 0.56°C deviation in the surface temperature changes the naphthalene vapor density at the surface by as much as 6%. The measured temperatures varied within this range during a test run of one to two hour duration. The change of surface elevation ranged from 0.05 to 0.2 mm in most of the test runs. The bulk naphthalene vapor density at the test channel exit

is found to be between 18% to 25% of the wall naphthalene vapor density, depending on the Reynolds number. In calculating the uncertainty for the bulk density at a certain streamwise location, a maximum deviation of 5% of the wall density from the linearly interpolated value is estimated. Based on the method in Kline and McClintock [1953], the maximum uncertainty for the Sherwood number is estimated to be 10.8%, which occurs at the test channel exit. The uncertainty for the Reynolds number is found to be 4.8%.

DISCUSSION OF RESULTS

To investigate the Reynolds number effect with and without rotation, tests with three different Reynolds numbers of 5,500, 10,000, and 14,500 are conducted under the stationary condition and for $Ro = 0.09$. To study the rotation number effect, rotation number is varied up to 0.24 while the Reynolds number is maintained at 5,500. In this section, the spanwise averaged or regionally averaged Sherwood number ratios on the leading and trailing walls will be presented along a streamwise coordinate, Z/D. Along the two straight passes of the test section ($0 \leq Z/D \leq 7$ and $9.5 \leq Z/D \leq 16.5$), the local Sherwood number ratios at nine spanwise distributed measurement points at a given Z/D are averaged to obtain the spanwise averaged value. In the turn, the local Sherwood number ratios are averaged over three regions: 36 distributed measurement points in an upstream square region with an area of D^2, 24 points in a middle rectangular region with an area of $0.5D^2$, and 36 points in a downstream square region with an area of D^2. These regions are considered to be located at $Z/D = 7.5$, 8.25, and 9.0. In addition, two selected normalized local Sherwood number contours on the leading and trailing walls will be presented.

Stationary Channel

The streamwise variation of the Sherwood number ratio for $Re = 10{,}000$ is given in Fig. 3. Without

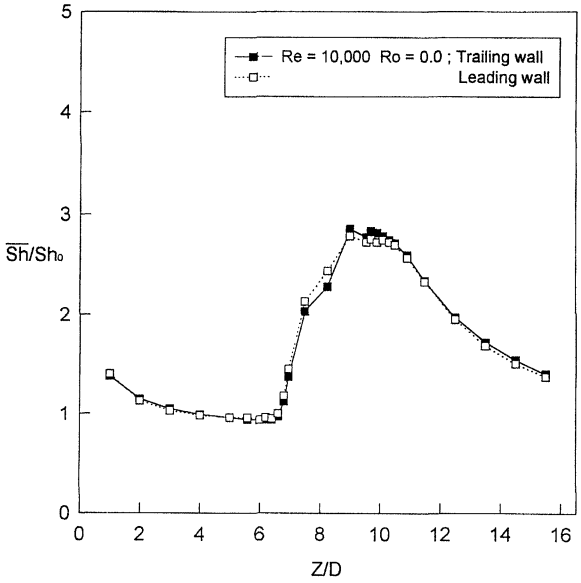

FIGURE 3 Streamwise variation of $\overline{Sh}/Sh_0$ for $Re = 10{,}000$ and $Ro = 0.0$.

rotation, the flow through the two-pass channel should be symmetrical with respect to the midplane between the leading and trailing walls. The figure shows that there are very small variations between the mass transfer distributions on the two walls. The variations are well within the estimated uncertainty.

In the first pass, the value of the Sherwood number ratio decreases monotonically along the streamwise direction to about 1.0 near the turn. Thus, the velocity field as well as the naphthalene vapor concentration field may be considered fully developed entering the turn. As the flow enters the turn, the value of $\overline{Sh}/Sh_0$ begins to increase sharply. Around the turn, the Sherwood number ratio increases from 2.0 to its peak value of about 2.8.

Immediately downstream of the turn, between $Z/D = 9.5$ and 10.5, the values of the spanwise averaged Sherwood number ratio remain quite high, and are only slightly lower than the peak value in the turn (at $Z/D = 9.0$). Along the second straight pass, $\overline{Sh}/Sh_0$ decreases monotonically, as the flow redevelops. The increased turbulence level due to the turn results in higher mass transfer in the second pass than in the first pass.

The corresponding normalized local Sherwood number distributions on the leading and trailing walls are given in Fig. 4. The distributions show that the local mass transfer is the highest along the outer edge of each of the two principal walls, downstream of the second outer corner of the turn. At the entrance of the turn, the main flow bends toward the tip of the inner wall due to the large abrupt pressure increase that balances the turn-induced centrifugal force field. A relatively low mass transfer region at the first outer corner of the turn is evident, indicating flow recirculation at the corner. The main flow continues toward the end wall at an angle, impinges on the end wall, and glides along the downstream portion of the end wall. The flow then negotiates around the second outer corner of the turn, and impinges on the outer wall in the second pass. The deflection of this flow toward the principal walls causes the high mass transfer at the second outer corner of the turn on each of the principal walls.

The local Sherwood number distributions in Fig. 4 also show a relatively high mass transfer region on each of the principal walls near the inner wall downstream of the tip of the inner wall due to the deflection of the reattached flow on the inner wall toward the two principal walls. Thus, the spanwise averaged Sherwood number ratio remains quite high immediately downstream of the turn, between $Z/D = 9.5$ and 10.5, as shown in Fig. 3.

Effect of Reynolds Number, Stationary Channel

Figure 5 compares the spanwise averaged Sherwood number distributions with no rotation for three Reynolds numbers: 5,500, 10,000, and 14,500. Around the turn, the Sherwood number ratio increases as the Reynolds number is decreased. As the Reynolds number is decreased from 10,000 to 5,500, the Sherwood number ratio increases markedly in the turn and in the upstream half of the second pass. In the first pass and in the downstream portion of the second pass, the effect of varying Re on $\overline{Sh}$ is well absorbed by the introduction of the normalizing factor, Sh_0, which has a 0.8 power dependency on Re. Thus, the Sherwood number in the turn is a weaker function of the Reynolds number relative to that for flow through a straight channel.

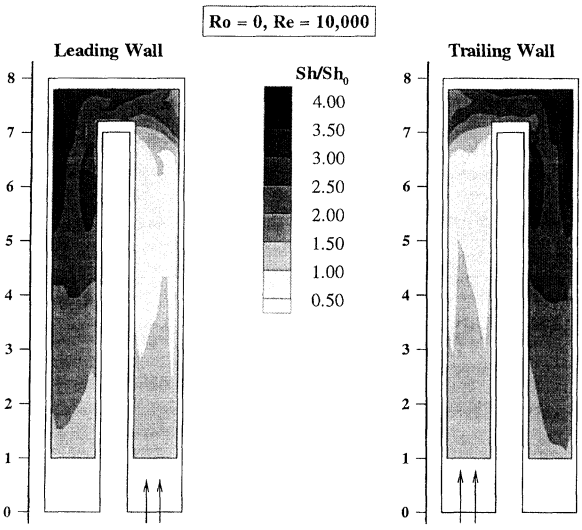

FIGURE 4 Local mass transfer distribution in a stationary channel, $Re = 10{,}000$.

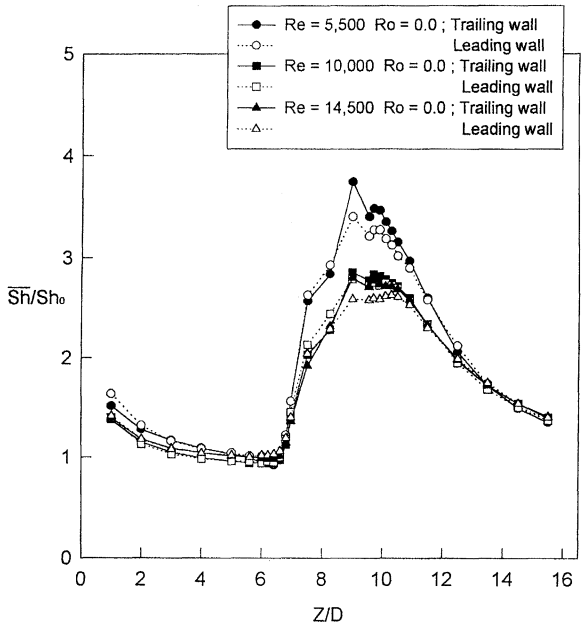

FIGURE 5 Effect of Reynolds number on mass transfer in a stationary channel.

The turn-induced centrifugal force pushes the core flow toward the end wall and the outer wall downstream of the second outer corner in the turn, generating a strong pressure gradient with high pressures near the end wall and the downstream outer side wall. The low momentum flow near the two principal walls is forced by the pressure field to move from the outer walls toward the tip of the inner wall, forming double cellular vortices. The double vortices are primarily responsible for the high mass transfer in the turn as they promote mixing of the core flow with the highly concentrated near-wall flow. The strength of the secondary flow near the two principal walls depends on the pressure field and the degree of momentum deficit near the two walls. If the ratio of the centrifugal force and the force that results from the pressure field remains about the same and is independent of the Reynolds number, the secondary flow should be strengthened when the Reynolds number is decreased. For the 180° turn with sharp corners, the local flow phenomena such as flow impingement, separation, recirculation, and reattachment may further contribute to the weak dependency (that is, less than a 0.8 power) of the Sherwood number on the Reynolds number. The aforementioned reasoning may be applied to explain why the Sherwood number ratio is higher in the turn and in the region immediately downstream of the turn in the second pass, when the Reynolds number is reduced.

Comparison with Published Results

In Fig. 6, the mass transfer results in the present study are compared with published heat transfer results from three prior studies. Although all of the test channels in these prior studies had a square flow cross section, the geometries of the test channels (the lengths of the entrance channels, the lengths of the straight passes, the corners of the turns, and the thicknesses of the inner walls) and the test conditions (the Reynolds numbers and the wall heating conditions) are different from those in the present study to various degrees. Table I lists the test section geometries and the test conditions

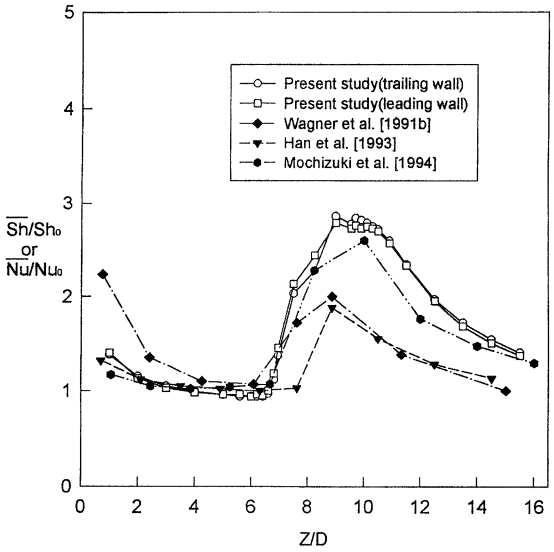

FIGURE 6 Comparison of results of present study with those from prior studies.

TABLE I Test conditions and geometries of test channels in this study verus those of three prior studies

	Re	Thermal boundary condition	Unheated entrance length	Heated length of first straight pass	Thickness of inner wall	Radius of inner wall tip
Present study	10,000	Constant temperature*	10*D*	7*D*	0.5*D*	0
Wagner et al. [1991b]	25,000	Constant temperature	1*D*	14*D*	2.4*D*	1*D*
Han et al. [1993]	10,000	Constant temperature or constant heat flux	24*D*	10*D*	1*D*	0.5*D*
Mochizuki et al. [1994]	20,000	Constant heat flux	30*D*	10*D*	0.7*D*	0.2*D*

* Naphthalene mass transfer experiment.

of the test runs from these studies that are selected for comparison.

To compare the heat/mass transfer distributions along the first straight pass, the published data of Wagner et al. [1991b], Han et al. [1993], and Mochizuki et al. [1994] are plotted in Fig. 6 with modified streamwise coordinates: the streamwise coordinate, Z/D, at the upstream and downstream ends of the first straight pass are assigned values of 0.0 and 7.0, respectively. For instance, since the length of the first pass of the test section in Wagner et al. [1991b] was 14 times the hydraulic diameter, the actual values of Z/D for their data were twice the values shown in Fig. 6. Also, the data of Mochizuki et al. [1994] are normalized using the correlation, $Nu_0 = 0.023\, Re^{0.8}\, Pr^{0.4}$, instead of $0.022\, Re^{0.8}\, Pr^{0.5}$ that was used in their study. Changing the correlation gives values that are about 8% lower than the published values.

The present data for the first straight pass are within 10% of those from Han et al. [1993] and Mochizuki et al. [1994]. The data from Wagner et al. [1991b] are much higher than those from the other three studies since their unheated starting length was only one hydraulic diameter long such that the developing velocity profile was quite different from those in the other three studies.

In the turn and in the second pass, the present data are higher than those from Mochizuki et al. [1994], which, in turn, are much higher than those from Wagner et al. [1991b] and Han et al. [1993]. For flow around a bend, the turn-induced centrifugal and Coriolis forces, which drive secondary flows and enhance turbulence mixing at the turn, are known to decrease as the radius of curvature of the bend increases. In the present study and in Mochizuki et al. [1994], the thicknesses of the inner walls and the tip radii are smaller than those of Wagner et al. [1991b] and Han et al. [1993]. For flow around a sharp turn with sharp corners, the separated flow at the tip of the inner wall may enhance turbulence mixing further in the downstream portion of the turn, causing very high overall heat/mass transfer over a region that extends from the end wall to the upstream portion of the second pass. Thus, a sharp turn with sharp corners such as the one in the test channel of this study enhances the heat/mass transfer in the turn and in the second pass more than a smooth turn with rounded corners.

The present study yields results that are quite consistent with those of Mochizuki et al. [1994], in which the turn geometry was very similar to the sharp turn of the present study. Note that a constant heat flux thermal boundary condition was employed in Mochizuki et al. [1994], while in the present study, the boundary condition corresponds to that of constant wall temperature. Han et al. [1993] reported that for a stationary two-pass square channel, the Nusselt numbers for the two thermal boundary conditions should be within 5% of one another. Note also that the heat transfer data reported in Mochizuki et al. [1994] are for streamwise locations along the centerlines of the two principal walls.

Effect of Rotation Number, Rotating Channel

To examine the effect of rotation, the rotational speed is varied while the main flow rate is maintained constant. Figure 7 shows the effect of varying the rotation number from 0.0 to 0.24 on the streamwise $\overline{Sh}/Sh_0$ distribution, with $Re = 5{,}500$. In the first pass, the mass transfer on the trailing wall increases with increasing rotation number, while that on the leading wall decreases. At $Ro = 0.24$, the value of $\overline{Sh}/Sh_0$ near the downstream end of the first straight pass increases by about 60% on the trailing wall, and decreases by 65% on the leading wall, compared with the corresponding stationary value. The rotation-induced Coriolis force in the radially outward flow pushes the high momentum core fluid toward the trailing wall with an accompanying pressure gradient across the channel cross section, and the pressure field drives the low momentum fluid near the inner and outer walls toward the leading wall, forming double vortices. The higher mass transfer on the trailing wall and lower mass transfer on the leading wall are primarily due to the shift of the

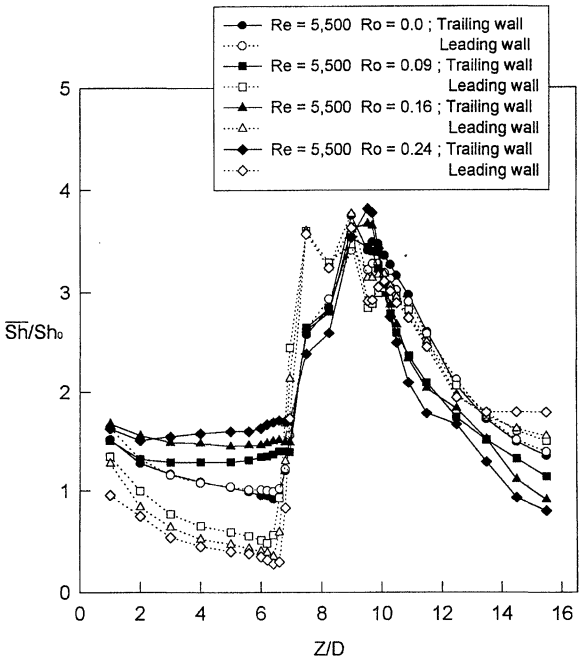

FIGURE 7 Effect of rotation number on mass transfer.

high velocity, low concentration core flow toward the trailing wall, causing large velocity and concentration gradients near the trailing wall. For an unheated rotating duct, Johnston et al. [1972] showed experimentally that a stabilization process occurs near the leading wall, resulting in the suppression of turbulence, and increasing further the difference between the mass transfer on the trailing wall and that on the leading wall in the first pass.

The leading wall average mass transfer with rotation increases abruptly in the upstream portion of the turn region (at $Z/D = 7.5$). The $\overline{Sh}/Sh_0$ value is much higher than that in the same turn region in the stationary channel case, and is as high as the peak value in the downstream portion of the turn (at $Z/D = 9.0$) in the stationary channel case. The leading wall average mass transfer with rotation is lower in the middle portion of the turn (at $Z/D = 8.25$) than in the upstream and downstream portions of the turn. Note that $\overline{Sh}/Sh_0$ increases in the streamwise direction around the turn in the stationary channel case. The average mass transfer in the downstream portion of the turn in a rotating channel is about the same as that in a stationary channel.

In the region immediately downstream of the turn, between $Z/D = 9.5$ and 13.5, the shapes of the leading wall $\overline{Sh}/Sh_0$ distributions with and without rotation are similar. The leading wall $\overline{Sh}/Sh_0$ values with and without rotation are about the same, except that the $\overline{Sh}/Sh_0$ values in the rotating channel cases are slightly lower than the corresponding stationary channel values at the turn exit.

On the trailing wall, the $\overline{Sh}/Sh_0$ distributions with rotation are similar to that in the stationary channel case in the turn. At the highest rotation number of 0.24, the $\overline{Sh}/Sh_0$ values are lower than those in the other cases. Immediately downstream of the turn in the second pass, the trailing wall mass transfer with rotation is generally lower than that in a stationary channel, except for a small increase at the exit of the turn at the higher rotation numbers of 0.16 and 0.24.

The shapes of the mass transfer distributions on both the leading and trailing walls at the turn and immediately downstream of the turn remain almost invariant with respect to the rotation number, for the Ro values between 0.09 and 0.24, indicating the strong dependency of the flow field on the geometry of the sharp turn. The sole effect of rotation is evident only after $4D$ downstream of the turn exit ($Z/D > 13.5$). The reversed rotational secondary flow in the radial inward flow increases the leading wall mass transfer and decreases the trailing wall mass transfer.

Figure 8 presents the local Sherwood number ratio contours for $Ro = 0.24$ and $Re = 5{,}500$. The figure shows that the leading wall mass transfer is very high along the end wall and is low near the tip of the inner wall in the turn. There is a high mass transfer region on the leading wall along the outer wall downstream of the second outer corner of the turn, which is similar to that in a stationary channel. On the trailing wall, the mass transfer in the upstream portion of the turn is relatively low and the high mass transfer zone along the outer wall downstream of the second outer corner of the turn merges toward the second outer corner.

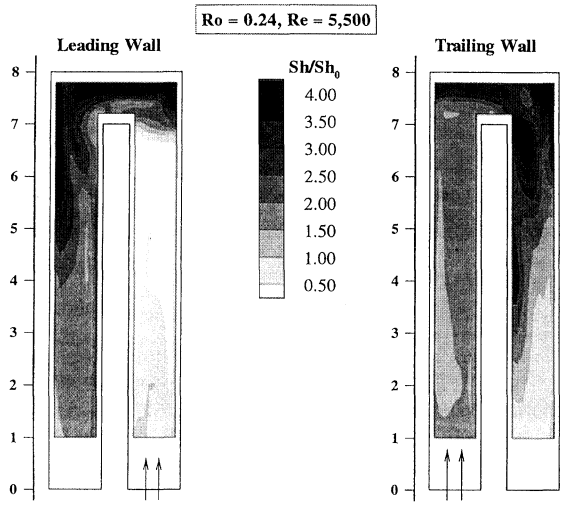

FIGURE 8 Local mass transfer distribution in a rotating channel, $Re = 5{,}550$ and $Ro = 0.24$.

With no rotation, the separated flow at the tip of the inner wall reattaches on the inner wall downstream of the turn exit. There exists an isolated relatively high mass transfer region on each of the leading and trailing walls near the reattachment region (see Fig. 4). With rotation, the high mass transfer region on the trailing wall intensifies and moves much closer to the second inner corner of turn, and that on the leading wall is reduced and is replaced by a low mass transfer region along the downstream side of the inner wall (see Fig. 8).

Figure 8 also shows that, along the first pass, the mass transfer is much higher on the trailing wall and much lower on the leading wall than that in a stationary channel, as a result of rotation. The combined effect of the turn and rotation is evident over a significant portion of the second pass.

The local mass transfer contours help to show the higher average mass transfer in the upstream portion of the turn on the leading wall than on the trailing wall, and the initially higher and subsequently lower mass transfer on the trailing wall immediately downstream of the turn.

As the flow approaches the turn, the turn-induced pressure distribution causes the flow along the outer wall to decelerate. The rotation-induced vortex pair that is symmetrical in the first straight pass becomes unbalanced, as the outer vortex is strengthened in this low momentum flow region. At the turn entrance, the turn-induced vortex pair begins to emerge. This vortex pair is asymmetric due to the shift of the maximum velocity toward the trailing side by the rotational Coriolis force. The interaction between the rotation-induced vortex pair and the turn-induced vortex pair significantly strengthens the vortex nearer the leading wall in the upstream half of the turn region. This vortex forces the outer portion of core flow toward the leading wall, causing a large increase of the mass transfer along the outside edge of the leading wall.

The aforementioned much-intensified vortex is believed to increase the mass transfer throughout the turn region as it causes vigorous mixing of the bulk flow. This vortex also weakens the local flow phenomena such as the separated flow on the outer wall near the turn entrance, which would otherwise take place in the stationary case due to the turn-induced pressure gradient.

As the flow passes through the downstream half of the turn, the rotation-induced vortex pair reappears, circulating in a reversed direction due to the radial inward mainstream. This vortex pair is unbalanced from the start due to the maximum velocity shift toward the outer wall that is caused by the centrifugal force of the turn. The already existing vortices mix with the emerging rotational vortices, resulting in a strong inner vortex and a weak outer vortex at the turn exit. The inner portion of the core flow is now driven toward the trailing wall. This intensified inner vortex sweeps the separated flow at the tip of the inner wall toward the trailing wall, increasing the mass transfer on the trailing wall downstream of the second inner corner of the turn.

Effect of Reynolds Number, Rotating Channel

In Fig. 9, the average Sherwood number ratio distributions with $Re = 5{,}500$, 10,000, and 14,500 at fixed $Ro = 0.09$ are given to examine the Reynolds number effect with rotation. The patterns of the

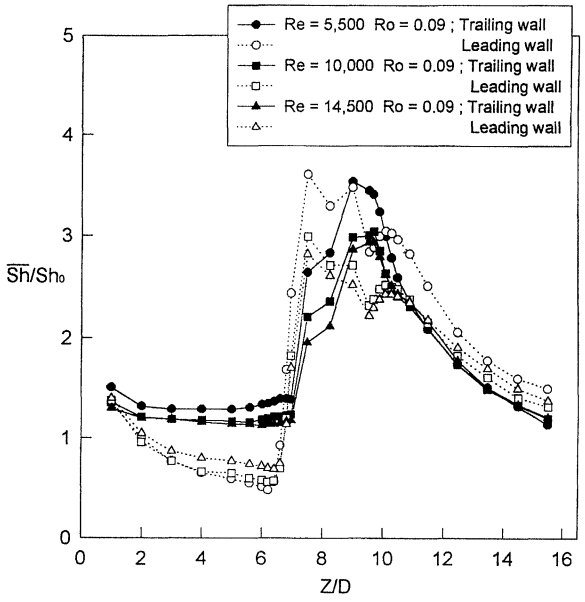

FIGURE 9 Effect of Reynolds number on mass transfer in a rotating channel.

$\overline{Sh}/Sh_0$ distributions on the leading and trailing walls are basically the same regardless of the Reynolds number, following the trends discussed in the previous section.

In the turn and immediately downstream of the turn, the Sherwood number ratio increases with decreasing Reynolds number, which is the same as that in the stationary channel case. The Reynolds number effect that is unique in the rotating channel case is evident in the first pass, where the difference between the Sherwood number ratio on the leading wall and that on the trailing wall becomes greater as the Reynolds number decreases. For a given rotation number, with a fixed ratio of the Coriolis and inertial forces, the strength of the secondary flow is determined by the degree of momentum deficit in the near wall boundary layer relative to the inertial force. Therefore, secondary flow due to the rotational Coriolis force strengthens when the main flow rate is reduced.

The aforementioned Reynolds number effect with rotation is not evident in the second pass, in which the rotational effect is coupled with the turn effect.

CONCLUDING REMARKS

An experimental study has been conducted to determine the regional mass transfer distribution for turbulent air flow in a rotating two-pass square channel with smooth walls. The effects of varying the Reynolds number and the rotation number on the spanwise averaged or regionally averaged mass transfer distribution were examined. The following conclusions are drawn:

Stationary Channel

1. Flow around a sharp turn with sharp corners causes larger mass transfer increase in the turn and in the second pass than flow around a smooth turn.
2. The normalized average Sherwood numbers in the turn and immediately downstream of the turn increase with decreasing Reynolds number.
3. The regional mass transfer increases along the streamwise direction in the turn and remains quite high immediately downstream of the turn in the second pass.

Rotating Channel

1. With radially outward flow in the first pass, increasing the rotation number increases the mass transfer on the trailing wall and decreases the mass transfer on the leading wall. It is caused by the rotational Coriolis force that shifts the high velocity, low concentration core flow toward the trailing wall, and flow stabilization near the leading wall.
2. There is an abrupt increase of the regional mass transfer with rotation in the upstream portion of the turn on the leading wall. The regional mass transfer on the trailing wall, however, increases along the streamwise direction in the turn, following the trend in the stationary channel case.
3. In the turn and immediately downstream of the turn, the shape of the $\overline{Sh}/Sh_0$ distribution is invariant over the range of rotation number between 0.09 and 0.24.

4. Many of the significant changes of the mass transfer in the turn and immediately downstream of the turn may be explained by the superposing effect of the turn-induced vortices and the rotation-induced vortices.
5. After $4D$ downstream from the turn exit, the rotational Coriolis force increases the leading wall mass transfer and decreases the trailing wall mass transfer in the second pass.
6. The difference between the $\overline{Sh}/Sh_0$ values on the leading and trailing walls in the first pass increases with decreasing Reynolds number. The values of $\overline{Sh}/Sh_0$ in the turn and immediately downstream of the turn increase with decreasing Reynolds number.

Acknowledgments

This research was sponsored by Energy Resources Center, College Station, Texas.

NOMENCLATURE

C_m	cumulative mass of naphthalene in air stream, [kg/s]
D	channel hydraulic diameter, [m]
h_m	local mass transfer coefficient, [m/s]
$\dot{m}''$	local mass flux of naphthalene, [kg/(m^2 · s)]
$\dot{M}$	mass flow rate of air, [kg/s]
Nu	local Nusselt number
$\overline{Nu}$	spanwise averaged Nusselt number
Nu_0	Nusselt number for fully developed flow
Pr	Prandtl number of air
$\dot{Q}$	volumetric flow rate of air, [m^3/s]
Re	Reynolds number based on channel hydraulic diameter
Ro	Rotation number
Sc	Schmidt number of naphthalene in air
Sh	local Sherwood number
$\overline{Sh}$	spanwise averaged Sherwood number
Sh_0	Sherwood number for fully developed flow
U	average air velocity, [m/s]
Δt	duration of test run, [s]
Δz	elevation change of naphthalene surface, [m]
Λ	diffusion coefficient of naphthalene, [m^2/s]
μ	dynamic viscosity of air, [N · s/m^2]
ν	kinematic viscosity of air, [m^2/s]
Ω	angular velocity, [rad/s]
ρ	density of air, [kg/m^3]
ρ_b	bulk naphthalene vapor density, [kg/m^3]
ρ_s	density of solid naphthalene, [kg/m^3]
ρ_w	naphthalene vapor density at wall, [kg/m^3]

References

Ambrose, D., Lawrenson, I.J. and Sprake, C.H.S. (1975) The Vapor Pressure of Naphthalene, *Journal of Chem. Thermodynamics*, Vol. 7, pp. 1173–1176.

Burggraf, F. (1970) Experimental Heat Transfer and Pressure Drop With Two-Dimensional Turbulence Promoter Applied to Two Opposite Walls of A Square Tube, in *Augmentation of Convection Heat Mass Transfer*, Eds.A.E. Bergles and R.L. Webb, pp. 70–79, ASME, New York.

Chandra, P.R., Han, J.C. and Lau, S.C. (1988) Effect of Rib Angle on Local Heat/Mass Transfer Distribution in a Two Pass Rib Roughened Channel, *ASME Journal of Turbomachinery*, Vol. 110, pp. 233–241.

Chyu, M.K. (1991) Regional Heat Transfer in Two-Pass and Three-Pass Passages With 180-Deg Sharp Turns, *ASME Journal of Heat Transfer*, Vol. 113, pp. 63–70.

Donne, D. and Meyer, L. (1977) Turbulent Convective Heat Transfer from Rough Surfaces With Two Dimensional Rectangular Ribs, *International Journal of Heat and Mass Transfer*, Vol. 20, pp. 582–620.

Fan, C.S. and Metzger, D.E. (1987) Effects of Channel Aspect Ratio on Heat Transfer in Rectangular Passage Sharp 180-Deg Turns, ASME Paper No. 87-GT-113.

Goldstein, R.J. and Cho, H.H. (1995) A Review of Mass Transfer Measurements Using Naphthalene Sublimation, *Experimental Thermal and Fluid Science*, Vol. 10, pp. 416–434.

Guidez, J. (1988) Study of Convective Heat Transfer in Rotating Coolant Channel, ASME Paper No. 88-GT-33.

Han, J.C., Chandra, P.R. and Lau, S.C. (1988) Local Heat/Mass Transfer Distributions Around Sharp 180-Deg Turns in Two-Pass Smooth and Rib-Roughened Channels, *ASME Journal of Heat Transfer*, Vol. 110, pp. 91–98.

Han, J.C., Zhang, Y.M. and Kalkuehler, K. (1993) Uneven Wall Temperature Effect on Local Heat Transfer in a Rotating Two-Pass Square Channel With Smooth Walls, *ASME Journal of Heat Transfer*, Vol. 115, pp. 912–920.

Han, J.C., Zhang, Y.M. and Lee, C.P. (1991) Influence of Surface Heat Flux Ratio on Heat Transfer Augmentation in Square Channels With Parallel, Crossed and V-Shaped Angled Ribs, ASME Paper No. 91-GT-3.

Iskakov, K.M. and Trushin, V.A. (1985) Influence of Rotation on Heat Transfer in a Turbine-Blade Radial Slot Channel, *Thermal Engineering*, Vol. 32, pp. 52–55.

Johnston, J.P., Halleen, R.M. and Lezius, D.K. (1972) Effects of Spanwise Rotation on the Structure of Two-Dimensional Fully Developed Turbulent Channel Flow, *Journal of Fluid Mechanics*, Vol. 56, pp. 533–557.

Karni, J. and Goldstein, R.J. (1990) Surface Injection Effect on Mass Transfer from a Cylinder in Crossflow: A Simulation of Film Cooling in the Leading Edge Region of a Turbine Blade, *ASME Journal of Turbomachinery*, Vol. 112, pp. 418–427.

Kline, S.J. and McClintock, F.A. (1953) Describing Uncertainties in Single Sample Experiments, *Mechanical Engineering*, Vol. 75, pp. 3–8.

Kukreja, R.T., Lau, S.C. and McMillin, R.D. (1993) Local Heat (Mass) Transfer Distribution in a Square Channel with Full and V-Shaped Ribs, *International Journal of Heat and Mass Transfer*, Vol. 36, pp. 2013–2020.

Lau, S.C., Kukreja, R.T. and McMillin, R.D. (1991a) Effects of V-Shaped Rib Arrays on Turbulent Heat Transfer and Friction of Fully Developed Flow in a Square Channel, *International Journal of Heat and Mass Transfer*, Vol. 34, pp. 1605–1616.

Lau, S.C., McMillin, R.D. and Han, J.C. (1991b) Turbulent Heat Transfer and Friction in a Square Channel With Discrete Turbulators, *ASME Journal of Turbomachinery*, Vol. 113, pp. 360–366.

Lau, S.C., McMillin, R.D. and Han, J.C. (1991c) Heat Transfer Characteristics of Turbulent Flow in a Square Channel With Angled Discrete Ribs, *ASME Journal of Turbomachinery*, Vol. 113, pp. 367–374.

McMillin, R.D. and Lau, S.C. (1994) Effect of Trailing-Edge Ejection on Local Heat (Mass) Transfer in Pin Fin Cooling Channels in Turbine Blades, *ASME Journal of Turbomachinery*, Vol. 116, pp. 159–168.

Metzger, D.E. and Sahm, M.K. (1986) Heat Transfer Around Sharp 180-Deg Turns in Smooth Rectangular Channels, *ASME Journal of Heat Transfer*, Vol. 108, pp. 500–506.

Mochizuki, S., Takamura, J., Yamawaki, S. and Yang, W.-J. (1994) Heat Transfer in Serpentine Passages with Rotation," *ASME Journal of Turbomachinery*, Vol. 116, pp. 133–140.

Sogin, H.H. (1958) Sublimation from Disks to Air Streams Flowing Normal to Their Surfaces, *Transactions of ASME*, Vol. 80, pp. 61–69.

Sparrow, E.M. and Tao, W.Q. (1983) Enhanced Heat Transfer in a Flat Rectangular Duct with Streamwise-Periodic Disturbances at One Principal Wall, *ASME Journal of Heat Transfer*, Vol. 105, pp. 851–861.

Wagner, J.H., Johnson, B.V., Graziani, R.A. and Yeh, F.C. (1991c) Heat Transfer in Rotating Serpentine Passages with Trips Normal to the Flow, ASME Paper No. 91-GT-265.

Wagner, J.H., Johnson, B.V. and Hajek, T.J. (1991a) Heat Transfer in Rotating Passages With Smooth Walls and Radial Outward Flow, *ASME Journal of Turbomachinery*, Vol. 113, pp. 42–51.

Wagner, J.H., Johnson, B.V., Steuber, G.D. and Yeh, F.C. (1992) Heat Transfer in Rotating Serpentine Passages With Trips Skewed to the Flow, ASME Paper No. 92-GT-191.

Wagner, J.H., Johnson, B.V. and Yeh, F.C. (1991b) Heat Transfer in Rotating Serpentine Passages With Smooth Walls, *ASME Journal of Turbomachinery*, Vol. 113, pp. 321–330.

Wagner, R.E. and Velkoff, H.R. (1972) Measurements of Secondary Flows in a Rotating Duct, ASME Paper No. 72-GT-17.

Webb, R.L., Eckert, E.R.G. and Goldstein, R.J. (1971) Heat Transfer and Friction in Tubes With Repeated Rib-Roughness, *International Journal of Heat and Mass Transfer*, Vol. 14, pp. 601–617.

MANEY
publishing

The Institute of Materials, Minerals & Mining

ENERGY MATERIALS

NEW FOR 2006

Materials Science & Engineering for Energy Systems

Maney Publishing on behalf of the Institute of Materials, Minerals and Mining

Economic and environmental factors are creating ever greater pressures for the efficient generation, transmission and use of energy. Materials developments are crucial to progress in all these areas: to innovation in design; to extending lifetime and maintenance intervals; and to successful operation in more demanding environments. Drawing together the broad community with interests in these areas, *Energy Materials* addresses materials needs in future energy generation, transmission, utilisation, conservation and storage. The journal covers thermal generation and gas turbines; renewable power (wind, wave, tidal, hydro, solar and geothermal); fuel cells (low and high temperature); materials issues relevant to biomass and biotechnology; nuclear power generation (fission and fusion); hydrogen generation and storage in the context of the 'hydrogen economy'; and the transmission and storage of the energy produced.

As well as publishing high-quality peer-reviewed research, *Energy Materials* promotes discussion of issues common to all sectors, through commissioned reviews and commentaries. The journal includes coverage of energy economics and policy, and broader social issues, since the political and legislative context influence research and investment decisions.

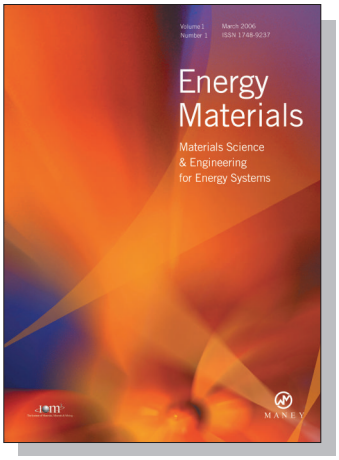

CALL FOR PAPERS

Contributions to the journal should be submitted online at **http://ema.edmgr.com**

To view the Notes for Contributors please visit: **www.maney.co.uk/journals/notes/ema**

Upon publication in 2006, this journal will be available via the Ingenta Connect journals service. To view free sample content online visit: **www.ingentaconnect.com/content/maney**

SUBSCRIPTION INFORMATION

Volume 1 (2006), 4 issues per year
Print ISSN: 1748-9237 Online ISSN: 1748-9245
Individual rate: £76.00/US$141.00
Institutional rate: £235.00/US$435.00
Online-only institutional rate: £199.00/US$367.00
For special IOM^3 member rates please email **subscriptions@maney.co.uk**

For further information please contact:
Maney Publishing UK
Tel: +44 (0)113 249 7481 Fax: +44 (0)113 248 6983 Email: subscriptions@maney.co.uk
or
Maney Publishing North America
Tel (toll free): 866 297 5154 Fax: 617 354 6875 Email: maney@maneyusa.com

For further information or to subscribe online please visit
www.maney.co.uk